BULLETIN OF THE POLISH ACADEMY OF SCIENCES
TECHNICAL SCIENCES, Vol. 72(1), 2024, Article number: e148440
DOI: 10.24425/bpasts.2024.148440

Fault diagnosis of electrical faults of three-phase induction motors using acoustic analysis

Adam GLOWACZ[1]*, Maciej SULOWICZ[1], Jaroslaw KOZIK[2], Krzysztof PIECH[2], Witold GLOWACZ[3], Zhixiong LI[4,5], Frantisek BRUMERCIK[6], Miroslav GUTTEN[7], Daniel KORENCIAK[7], Anil KUMAR[8], Guilherme Beraldi LUCAS[9], Muhammad IRFAN[10], Wahyu CAESARENDRA[4,11], and Hui LIU[12]

[1] Cracow University of Technology, Faculty of Electrical and Computer Engineering, Department of Electrical Engineering, ul. Warszawska 24, 31-155 Kraków, Poland
[2] AGH University of Krakow, Faculty of Electrical Engineering, Automatics, Computer Science and Biomedical Engineering, Department of Power Electronics and Energy Control Systems, al. A. Mickiewicza 30, 30-059 Kraków, Poland
[3] AGH University of Krakow, Faculty of Electrical Engineering, Automatics, Computer Science and Biomedical Engineering, Department of Automatic Control and Robotics, al. A. Mickiewicza 30, 30-059 Krakw, Poland
[4] Faculty of Mechanical Engineering, Opole University of Technology, Opole 45-758, Poland
[5] University of Religions and Denomina, Qom, Iran
[6] University of Zilina, Faculty of Mechanical Engineering, Department of Design and Machine Elements, Univerzitna 1, 010 26 Zilina, Slovakia
[7] University of Zilina, Faculty of Electrical Engineering and Information Technology, 8215/1 Univerzitna, 01026 Zilina, Slovakia
[8] Wenzhou University, College of Mechanical and Electrical Engineering, Wenzhou, 325 035, China
[9] Sao Paulo State University, Department of Electrical Engineering, Av. Eng. Luís Edmundo Carrijo Coube, 14-01, Bauru, Sao Paulo, Brazil
[10] Najran University Saudi Arabia, Electrical Engineering Department, College of Engineering, Najran 61441, Saudi Arabia
[11] Faculty of Integrated Technologies, Universiti Brunei Darusalam, Jalan Tungku Link, Gadong BE1410, Brunei
[12] China Jiliang University, College of Quality and Safety Engineering, Hangzhou 310018, China

Abstract. Fault diagnosis techniques of electrical motors can prevent unplanned downtime and loss of money, production, and health. Various parts of the induction motor can be diagnosed: rotor, stator, rolling bearings, fan, insulation damage, and shaft. Acoustic analysis is non-invasive. Acoustic sensors are low-cost. Changes in the acoustic signal are often observed for faults in induction motors. In this paper, the authors present a fault diagnosis technique for three-phase induction motors (TPIM) using acoustic analysis. The authors analyzed acoustic signals for three conditions of the TPIM: healthy TPIM, TPIM with two broken bars, and TPIM with a faulty ring of the squirrel cage. Acoustic analysis was performed using fast Fourier transform (FFT), a new feature extraction method called MoD-7 (maxima of differences between the conditions), and deep neural networks: GoogLeNet, and ResNet-50. The results of the analysis of acoustic signals were equal to 100% for the three analyzed conditions. The proposed technique is excellent for acoustic signals. The described technique can be used for electric motor fault diagnosis applications.

Keywords: acoustic signal; induction motor; fault; neural network.

1. INTRODUCTION

Electric motors are used in fans, turbines, pumps, power tools, electrical appliances, trains, trams, automobiles, mining, ironworks, etc. (Fig. 1). Induction motors are widely used in industry. They are inexpensive, robust, and reliable under various environmental conditions.

Induction motor failures can cause unplanned downtime, and loss of production, health, and money. This is a motivation for developing new fault detection techniques. Fault diagnosis techniques can prevent downtime and loss of money, production, and health. Various parts of the induction motor can be diagnosed: rotor, stator (electrical faults), rolling bearings, fan, insulation damage, and shaft (mechanical faults).

Fig. 1. Application of electrical motors – trains

*e-mail: adglow@agh.edu.pl

Manuscript submitted 2023-08-01, revised 2023-10-28, initially accepted for publication 2023-11-07, published in February 2024.

In this research paper, the authors present a fault diagnosis method for three-phase induction motors (TPIM) using acoustic signals. The authors presented an experimental setup. Acoustic analysis was performed using fast Fourier transform (FFT), MoD-7, and deep neural networks: GoogLeNet and ResNet-50.

The article consists of seven sections: 1. Introduction – The authors introduce the use of induction motors and diagnostic signals of induction motors. 2. Theoretical background – The authors discuss a review of work related to induction motor fault diagnosis. 3. Measurements of TPIM acoustic signals – The authors present the experimental setup and measurements of the analyzed faults of TPIM. 4. Proposed technique for analyzing acoustic signals – Acoustic signals were classified using FFT, MoD-7, digital filtration, GoogLeNet, and ResNet-50. 5. Results of acoustic signals analysis – The analysis of acoustic signals is presented. 6. Discussion – The authors present discussion. 7. Conclusions – The authors present their work in this article.

2. THEORETICAL BACKGROUND

The following diagnostic signals can be used for fault detection: Stator current [1, 2], vibration signal [1, 2], acoustic signal [2], magnetic flux [3, 4], and thermal image [5, 6]. Fault diagnosis based on acoustic signal analysis has been developed in the literature. Acoustic analysis is non-invasive, and it can be used for the detection of different faults. Acoustic sensors are low-cost. However, the limitations of acoustic analysis are the following: interference from other sources, it does not work in a vacuum, it cannot localize fault, and it can only detect the fault.

Acceleration signals and acoustic signals were analyzed [7]. A fault diagnosis experiment platform was established. A fault diagnosis model of axle box bearing was proposed. Chirplet transform and support vector machine were used for the analysis. The following states were analyzed: normal, inner-race fault, roller fault, and outer-race fault. Classification accuracy was in the range of 98.21%–100.00%. In the next paper, acoustic signals of the CR400 EMU Traction Motor were analyzed using cross wavelet transform and GoogleNet [8]. Bandpass filtering was used. The results show that GoogleNet achieves in the range of 89.66%–98.23% accuracy in fault classification. A fault diagnosis system using acoustic emission and machine learning techniques was presented in the paper [9]. The fault diagnosis of commercial drill tool CT10128 was presented. FFT, RMS, mean value, Kurtosis, Skewness, crest factor, margin factor, Variance, and median measure were used. The accuracy for the proposed machine learning model was 96.1%. A method of fault diagnosis based on acoustic emission signals of thrust ball bearings was presented [10]. It was based on a wavelet sparse convolutional neural network. Four different sizes of roller and four different sizes of seat were analyzed. The experimental results were incredibly good for the proposed approach.

Discriminant analysis using multi-view learning for bearing fault diagnosis was described in the next paper [11]. FFT, multi-view features, and KNN were used for the analysis. The results were good. The proposed approach can detect the bearing fault correctly. A new methodology for ventilator acoustic fault diagnosis was developed [12]. Two states of the ventilator were analyzed: fault, and no-fault. Spectrograms were computed. The convolutional neural network classified acoustic data. The accuracy of the proposed methodology was equal to 0.95. Railway track monitoring using acoustic signals is presented in the paper [13]. The microphone and GPS sensor were used for the acquisition of acoustic signals. The proposed approach was based on multilayer perceptron, artificial neural network, logistic regression, AdaBoost, and random forest. It achieved accuracy in the range of 96%–98.4%. Acoustic and vibration signals of a high-voltage circuit breaker were analyzed [14]. The proposed approach was based on an Adaptive neural fuzzy inference system. Five states of the high-voltage circuit breaker were analyzed. The accuracy of the proposed approach was in the range of 75% to 100%. Rolling bearing fault diagnosis using a Generative adversarial network and acoustic signals was described in the paper [15]. Crack sizes 3 mm to 12 mm were analyzed. The proposed approach was compared with SVM and CNN. Average classification accuracy was in the range of 99.79%–100%. Bearing fault detection using vibration and acoustic signals was developed [16]. Healthy bearing, inner race fault, outer race fault, and ball fault were analyzed. Multidomain feature extraction SVM, relative wavelet energy, time-spectral features extraction, and reduction with linear discriminant analysis methods were analyzed. The proposed methods achieved classification results above 96%. A fault diagnosis of diesel engine exhaust valve leakage was presented [17]. The proposed approach uses analysis of acoustic signals. Three methods margin disparity discrepancy, domain adversarial neural network, and deep adaptation network were proposed. The experimental analysis was exceptionally good. A fault diagnosis method for automobile power seats was developed [18]. The authors used a smartphone for the measurement of acoustic signals. Healthy automobile power seats and automobile power seats with worn screw states were analyzed. The proposed method was based on acoustic analysis and retrained SVM. The accuracy of the proposed method was in the range of 98.04%–99.62%. Acoustic-based fault diagnosis of induction motors was developed [19]. The bearing dataset and the gearbox dataset were analyzed. A multi-input convolutional neural network was used for the analysis of acoustic signals. Computed accuracy was in the range of 95.09%–99.95%. The fault diagnosis method of the flywheel bearing cage using acoustic signals was presented [20]. The proposed method is based on multi-parameter clustering. The following states were analyzed: normal, rubbing uneven, and lubrication. The accuracy of the method was equal to 99.33% for three flywheel states. Fault diagnosis of rolling bearing using acoustic analysis was described [21]. Feature extraction method AVMD-IMVO-MCKD was proposed. The proposed AVMD-IMVO-MCKD method extracts features of acoustic signals correctly. A review of vibration-based wear monitoring was presented [22]. Techniques of vibration-based fault diagnosis were also discussed. Convolutional neural networks for vibration-based bearing fault diagnosis of rotating machinery were presented [23]. Fault diagnosis of bearings of wind turbines was also described [24]. Vibration and acoustic signals were analyzed using a convolutional residual network.

3. MEASUREMENTS OF ACOUSTIC SIGNALS OF TPIM

Three identical TPIMs (550 W) were analyzed. The authors considered the electrical faults of the TPIMs. The authors analyzed the acoustic signals for three conditions of the TPIM: healthy TPIM, TPIM with two broken bars, and TPIM with a defective ring of the squirrel cage (Fig. 2).

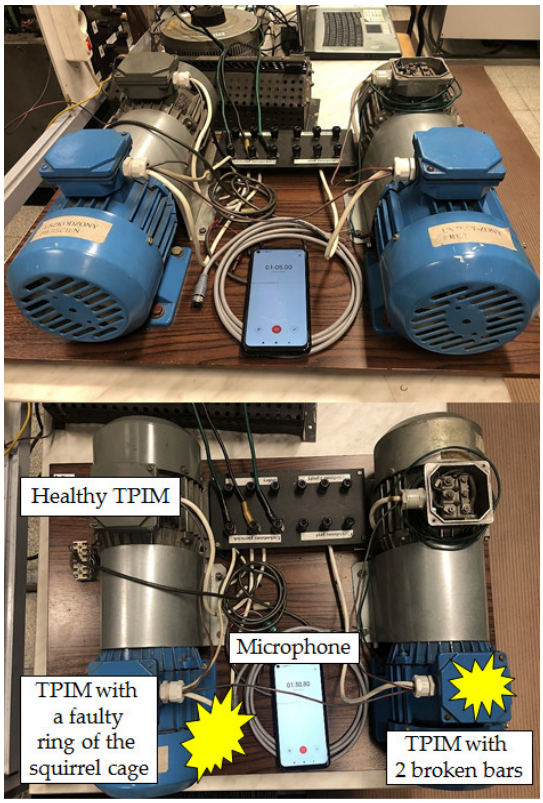

Fig. 2. Three-phase induction motors (550W)

Acoustic signals were recorded using a smartphone. In the research, the smartphone with a microphone was at 0.1 m from the motors. The format of the audio file was AAC, Advanced Audio Coding Format. The sampling frequency was 48 000 Hz. The spectra of the acoustic signals of the TPIM were presented (Figs. 3–5).

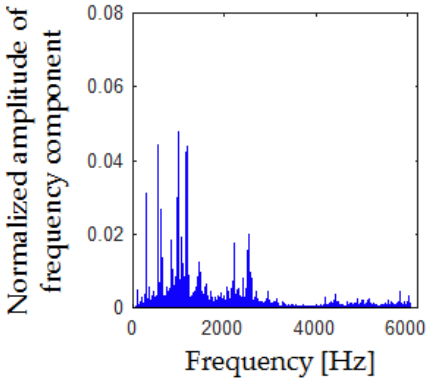

Fig. 3. Spectrum of the acoustic signal of the healthy TPIM

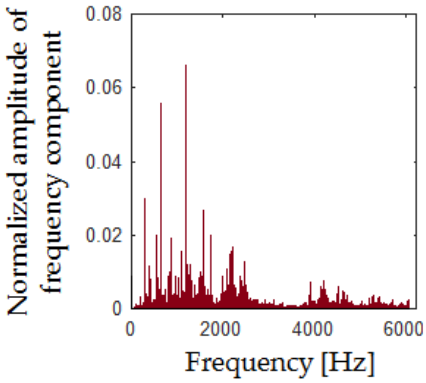

Fig. 4. Spectrum of the acoustic signal of the TPIM with two faulty rotor bars

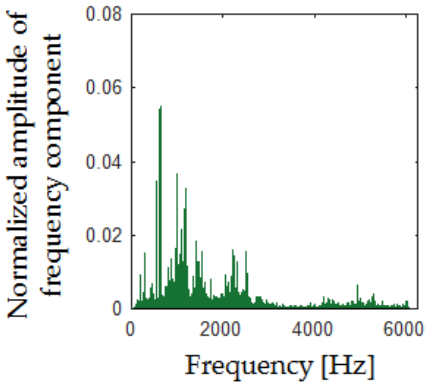

Fig. 5. Spectrum of the acoustic signal of the TPIM with a faulty ring of the squirrel cage rotor

4. PROPOSED TECHNIQUE FOR ACOUSTIC SIGNAL ANALYSIS

Acoustic signals were recorded using a smartphone. Subsequently, the acoustic data were split (1-second sample). Next, the FFT method was applied. The first approach of acoustic analysis is based on FFT, an original feature extraction method called MoD-7, GoogLeNet, and ResNet-50. FFT spectrum is computed. Differences between conditions are computed. Then, the band-pass filter (264–1784 Hz) is formed. The range of 264–1784 Hz was computed using MoD-7. The computed frequency components are converted into a matrix (39×39 pixels). The computed matrix is converted into a grayscale image ($224 \times 224 \times 3$). The computed grayscale images were used for training and testing GoogLeNet and ResNet-50.

The second approach is based on FFT and a low-pass filter (1–6084 Hz). The range of 1–6084 Hz was determined from the spectrum of the acoustic signals of the analyzed conditions visually. The computed frequency components are converted into a matrix (78×78 pixels). The computed matrix is converted into a grayscale image (224×224 pixels). The computed grayscale images were used for training and testing GoogLeNet and ResNet-50 (Fig. 6). MATLAB was used for the implementation of acoustic fault diagnosis.

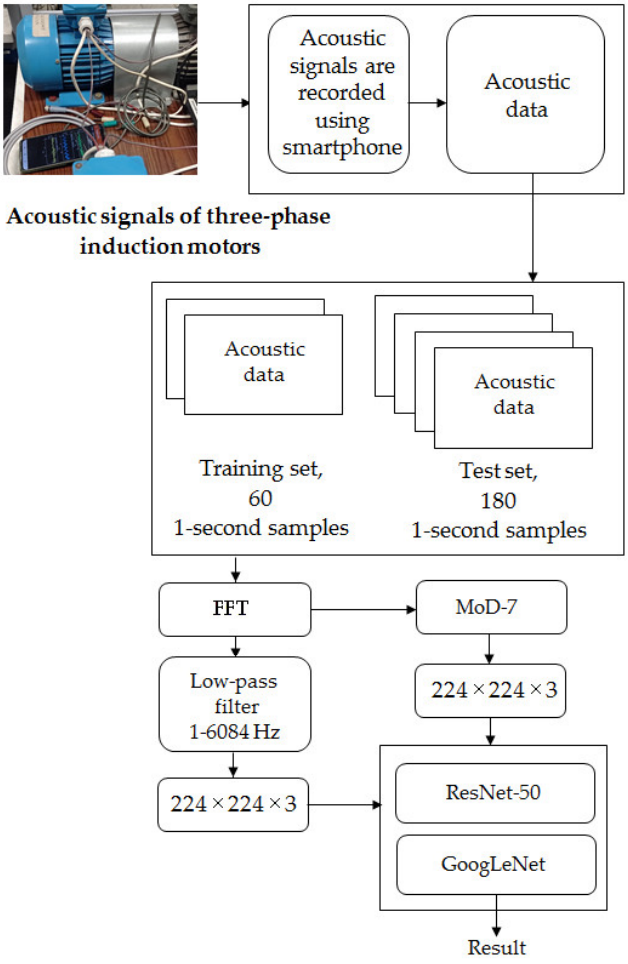

Fig. 6. The proposed fault diagnosis technique of the TPIM using acoustic signals

4.1. MoD-7

The MoD-7 method is proposed to extract features of acoustic signals. The MoD-7 has six steps of processing (Fig. 7):

1. Compute differences between FFT spectra: $x = |a - b|$, $y = |a - c|$, $z = |b - c|$, where a – FFT spectrum of healthy TPIM, b FFT spectrum of TPIM with two broken bars, c – FFT spectrum of TPIM with a faulty ring of the squirrel cage.
2. Compute seven maximal amplitudes of differences: x_{1m}, x_{2m}, x_{3m}, x_{4m}, x_{5m}, x_{6m}, x_{7m}, y_{1m}, y_{2m}, y_{3m}, y_{4m}, y_{5m}, y_{6m}, y_{7m}, z_{1m}, z_{2m}, z_{3m}, z_{4m}, z_{5m}, z_{6m}, z_{7m}.
3. Select the lowest (L_{freq}) and highest (H_{freq}) frequency of the computed maxima. For example, we found the following frequency components for $x = |a - b|$: 549, 650, 997, 998, 1149, 1198, 1199 Hz, and we found the following frequency components for $x = |b - c|$: 301, 601, 650, 998, 1079, 1199, 1572 Hz. The range 301–1572 Hz is selected.
4. Create a range of frequencies $\langle L_{\text{freq}} - t,\ H_{\text{freq}} + t\rangle$, where t is a number to create a square matrix. For example, L_{freq} = 100 Hz, H_{freq} = 990 Hz, then t = 5 Hz, ⟨95 Hz, 995 Hz⟩, because $30^2 = 900$. For example, L_{freq} = 100 Hz, H_{freq} = 1021 Hz, then t = 20 Hz (80 Hz, 1041 Hz), because $31^2 = 961$.
5. Select all frequency components in the range $\langle L_{\text{freq}} - t,\ H_{\text{freq}} + t\rangle$. For example 900 frequency components.
6. Compute a square matrix **S**, where **S** has all frequency components in the range $\langle L_{\text{freq}} - t,\ H_{\text{freq}} + t\rangle$. Matrix **S** is an image.

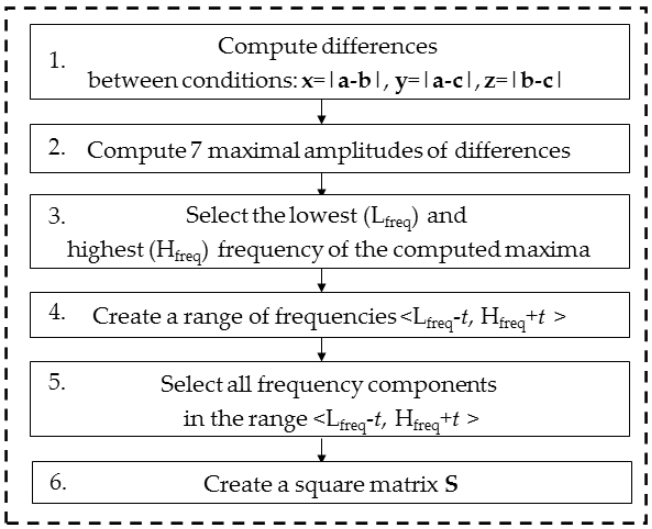

Fig. 7. The proposed MoD-7 method

The selection of the frequency range for seven maximal amplitudes of differences is presented in Figs. 8–10.

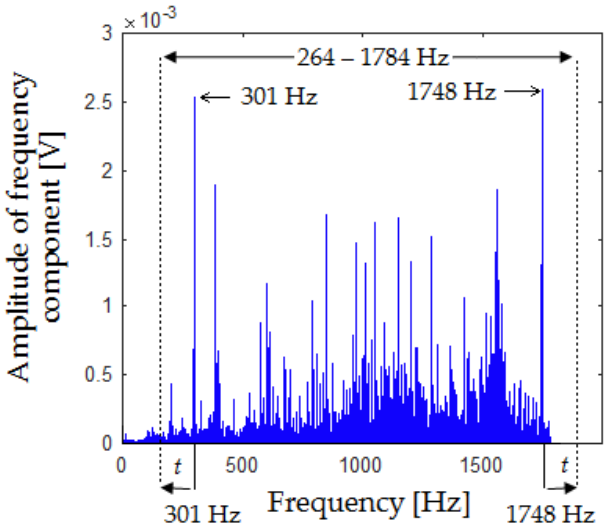

Fig. 8. Selection of the frequency range for seven maximal amplitudes of differences $|b - c|$

It can be noticed that the frequency range ⟨301 – 1748 Hz⟩ is selected for the analyzed acoustic data ($\langle L_{\text{freq}},\ H_{\text{freq}}\rangle$). Next parameter t = 37 Hz was computed (1748 – 301 = 1447, 1447 + 74 = 1521 = 39^2, t = 74/2 = 37). The frequency range $\langle L_{\text{freq}} - t,\ H_{\text{freq}} + t\rangle$ is equal to ⟨264 – 1785 Hz⟩ for analyzed acoustic data.

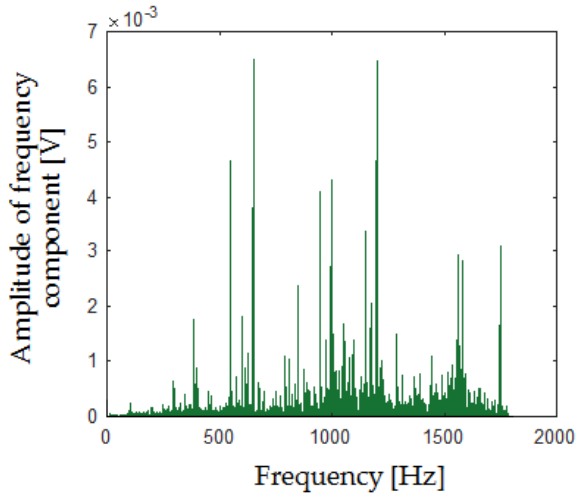

Fig. 9. Selection of the frequency range for seven maximal amplitudes of differences $|a-b|$

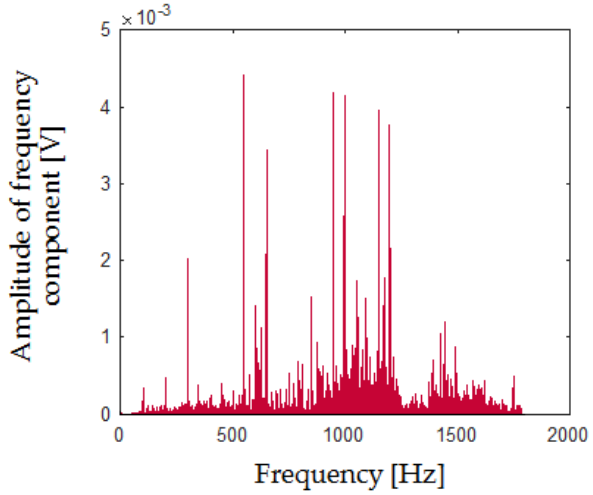

Fig. 10. Selection of the frequency range for seven maximal amplitudes of differences $|a-c|$

4.2. Features of the acoustic signal

The computed grayscale images ($224\times224\times3$, band-pass filter 264–1784 Hz, MoD-7) for three classes were presented in Fig. 11. Range of frequency 264–1784 Hz was computed using MoD-7.

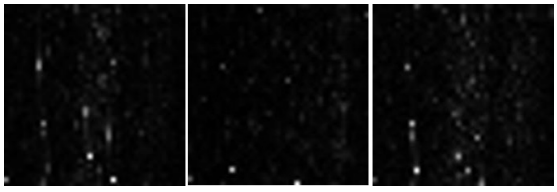

(a) (b) (c)

Fig. 11. a) Image of the acoustic signal (264–1784 Hz, MoD-7) of the healthy TPIM, b) Image of the acoustic signal of the TPIM with two faulty rotor bars, c) Image of the acoustic signal of the TPIM with a faulty ring of the squirrel cage

The computed grayscale images (224×224×3, low-pass filter 1–6084 Hz) for three classes were presented in Fig. 12.

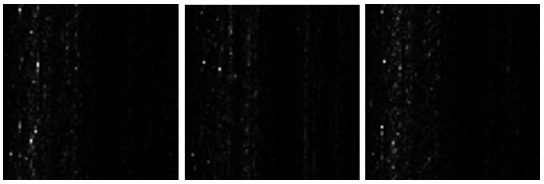

(a) (b) (c)

Fig. 12. (a) Image of the acoustic signal (1–6084 Hz) of the healthy TPIM; (b) Image of the acoustic signal of the TPIM with two faulty rotor bars; (c) Image of the acoustic signal of the TPIM with a faulty ring of the squirrel cage

White spots can be seen in Figs. 11 and 12. The analyzed images are different. The images in Fig. 11 are better distinguishable than those in Fig. 12.

4.3. GoogLeNet

GoogLeNet is a convolutional neural network. It was proposed in 2014. It has 22 deep layers. GoogLeNet was developed for image classification. It was trained for 1000 object categories. GoogLeNet requires input images of $224\times224\times3$ (RGB color). It also has an inception structure (nine inception modules). The inception structure processes the input images in parallel. Then each output result is merged. In the literature, GoogLeNet confirms high efficiency for image classification [25–28].

4.4. ResNet-50

ResNet-50 is a convolutional neural network. ResNet-50 was developed for image classification. It was proposed in 2016. ResNet-50 has 50 deep layers. ResNet-50 was trained for 1000 object categories. Input images of $224\times224\times3$ are required for ResNet-50 (RGB color). ResNet-50 has shortcut connections. Shortcut connections convert a neural network into a residual network. ResNet-50 has a bottleneck design. It uses three-layer bottleneck blocks. ResNet-50 stacks convolutional layers. Next, it skips some layers. After that, it uses the activations of the previous layer. Skipping some layers causes faster initial training of the ResNet-50. It is an extremely useful convolutional neural network [29–31]. There is also a possibility to use YOLO and other neural networks [32, 33].

5. RESULTS OF ANALYSIS OF ACOUSTIC SIGNALS

The analysis was conducted for three different conditions of the TPIM: healthy TPIM, TPIM with two broken bars, and TPIM with a faulty ring of the squirrel cage. Measurements were conducted for 60 seconds of each class. 60 training 1-second samples were used for training (20 1-second samples for each class). 180 test 1-second samples were used for the test (60 1-second samples for each class). The K-fold cross-validation method was used for the analysis. The efficiency of recognition – E_A is defined as (1):

$$E_A = 100\% * (CS_i)/(AS_i), \tag{1}$$

where CS – correctly recognized test samples for one i-th condition, AS – all test samples for one i-th condition, $i = 3$, in particular $i = 1$ for healthy TPIM, $i = 2$ for TPIM with two broken bars, $i = 3$ for TPIM with a faulty ring in the squirrel cage.

The arithmetic mean of E_A (AE_A) is expressed as (2):

$$AE_A = (E_{A1} + E_{A2} + E_{A3})/3, \tag{2}$$

where: $E_{A1} - E_A$ for healthy TPIM, $E_{A2} - E_A$ for TPIM with two broken bars, $E_{A3} - E_A$ for TPIM with a faulty ring of the squirrel cage.

Table 1 shows the results of the proposed technique using FFT, a band-pass filter (264–1784 Hz), MoD-7, GoogLeNet, and ResNet-50.

Table 1
Results of the proposed technique using FFT, a band-pass filter (264–1784 Hz), MoD-7, GoogLeNet, and ResNet-50

Condition of the TPIM	E_A [%]	
	GoogLeNet	ResNet-50
E_{A1}, healthy TPIM	100	95
E_{A2}, TPIM with two broken bars	100	100
E_{A3}, TPIM with a faulty ring of the squirrel cage	100	100
	AE_A [%]	
AE_A [%]	100	98.33

Table 2 shows the results of the proposed technique using FFT, low-pass filter (1–6084 Hz), GoogLeNet, and ResNet-50.

Table 2
Results of the proposed technique using FFT, low-pass filter (1-6084 Hz), GoogLeNet, and Res-Net-50

Condition of the TPIM	E_A [%]	
	GoogLeNet	ResNet-50
E_{A1}, healthy TPIM	100	100
E_{A2}, TPIM with two broken bars	100	100
E_{A3}, TPIM with a faulty ring of the squirrel cage	100	100
	AE_A [%]	
AE_A [%]	100	100

AE_A was in the range of 98.33–100% for the analyzed technique based on FFT, MoD-7, GoogLeNet, and ResNet-50 (Tables 1 and 2). The analyzed images were different. GoogLeNet and ResNet-50 work very well. The authors also analyzed ShuffleNet and MobileNet-V2. However, the results were not high for ShuffleNet and MobileNet-V2.

6. DISCUSSION

Acoustic analysis is non-invasive. Acoustic sensors are low-cost. Changes in the acoustic signal are often observed for faults in induction motors. Sometimes it can be detected using the human ear. Acoustic analysis is appropriate for electrical and mechanical faults.

However, the limitations of acoustic analysis are the following: interference from other sources, it does not work in a vacuum, it cannot localize fault, and it can only detect the fault. The proposed method MoD-7 works very well for the analyzed acoustic signals. Analyzed classes were limited to three.

However, the proposed approach can work for more classes. It depends on how much the acoustic signals differ from each other.

7. CONCLUSIONS

In this paper, the authors described the fault diagnosis method of three-phase induction motors (TPIM) using acoustic signals. The authors analyzed acoustic signals for three conditions of the TPIM: healthy TPIM, TPIM with two broken bars, and TPIM with a faulty ring of the squirrel cage. Acoustic signals of the TPIM were recorded using a smartphone. The position of the smartphone should be the same for all measurements. The proposed approach should also work for other positions of the smartphone. Similar electrical faults of motors can be detected.

Acoustic analysis was conducted for the Fast Fourier Transform (FFT), MoD-7, and deep neural networks: GoogLeNet, and ResNet-50. The results of recognition were 100%. The proposed techniques are excellent for acoustic signals.

In the future, the authors will develop new techniques of fault diagnosis. Future techniques will be based on various measurements: magnetic, acoustic, thermal, and electrical. More types of electrical motors and faults will be diagnosed. More parameters of electrical motors will be also analyzed.

FUNDING

The research was financed by a research subsidy from the Ministry of Education and Science of the Republic of Poland.

REFERENCES

[1] T. Garcia-Calva, D. Morinigo-Sotelo, V. Fernandez-Cavero, and R. Romero-Troncoso, "Early Detection of Faults in Induction Motors – A Review," *Energies*, vol. 15, p. 7855, 2022, doi: 10.3390/en15217855.

[2] C.Z. Liu, A. Cichon, G. Krolczyk, and Z.X. Li, "Technology development and commercial applications of industrial fault diagnosis system: a review," *J. Adv. Manuf. Technol.*, vol. 118, pp. 3497–3529, 2022, doi: 10.1007/s00170-021-08047-6.

[3] V. Gurusamy, G.A. Capolino, B. Akin, H. Henao, R. Romary, and R. Pusca, "Recent Trends in Magnetic Sensors and Flux-Based Condition Monitoring of Electromagnetic Devices". *IEEE Trans. Ind. Appl.*, vol. 58, no. 4, pp. 4668–4684, 2022, doi: 10.1109/TIA.2022.3174804.

[4] Z. Liu, G.Y. Tian, W. Cao, X. Dai, B. Shaw, and R. Lambert, "Non-invasive load monitoring of induction motor drives using magnetic flux sensor". *IET Power Electron.*, vol. 2, no. 2, pp. 189–195, 2017, doi: 10.1049/iet-pel.2016.0304.

[5] A. Glowacz, "Thermographic fault diagnosis of electrical faults of commutator and induction motors," *Eng. Appl. Artif. Intell.*, vol. 121, p. 105962, 2023, doi: 10.1016/j.engappai.2023.105962.

[6] A. Glowacz, "Ventilation diagnosis of minigrinders using thermal images," *Expert Syst. Appl.*, vol, 237, p. 121435, 2024, doi: 10.1016/j.eswa.2023.121435.

[7] J. Zhang, X. Hu, X. Zhong, and H. Zhou, "Fault Diagnosis of Axle Box Bearing with Acoustic Signal Based on Chirplet Transform and Support Vector Machine". *Shock Vibr.*, vol. 2022, p. 9868999, 2022, doi: 10.1155/2022/9868999.

[8] G. Yang, Y. Wei, and H. Li, "Acoustic Diagnosis of Rolling Bearings Fault of CR400 EMU Traction Motor Based on XWT and GoogleNet," *Shock Vibr.*, 2022, p. 2360067, 2022, doi: 10.1155/2022/2360067.

[9] R.R. Shubita, A.S. Alsadeh, and I.M. Khater, "Fault Detection in Rotating Machinery Based on Sound Signal Using Edge Machine Learning," *IEEE Access*, vol. 11, pp. 6665–6672, 2023, doi: 10.1109/ACCESS.2023.3237074.

[10] JY. Tai, C. Liu, X. Wu, and J. Yang, "Bearing fault diagnosis based on wavelet sparse convolutional network and acoustic emission compression signals," *Math. Biosci. Eng.*, vol 19, no. 8, pp. 8057–8080, 2022, doi: 10.3934/mbe.2022377.

[11] Z. Tong, W. Li, B. Zhang, H. Gao, X. Zhu, and E. Zio, "Bearing Fault Diagnosis Based on Discriminant Analysis Using Multi-View Learning," *Mathematics*, vol. 10, no. 20, p. 3889, 2022, doi: 10.3390/math10203889.

[12] G. Ciaburro, S. Padmanabhan, Y. Maleh, V. Puyana-Romero, "Fan Fault Diagnosis Using Acoustic Emission and Deep Learning Methods," *Informatics*, vol. 10, no. 1, p. 24, 2023, doi: 10.3390/informatics10010024.

[13] H.U.R. Siddiqui, A.A. Saleem, M.A. Raza, K. Zafar, K. Munir, and S. Dudley, "IoT Based Railway Track Faults Detection and Localization Using Acoustic Analysis," *IEEE Access*, vol. 10, pp. 106520–106533, 2022, doi: 10.1109/ACCESS.2022.3210326.

[14] Z. Chen, K. Zhang, L. Yang, and Y. Liang, "ANFIS based sound vibration combined fault diagnosis of high voltage circuit breaker (HVCB)," *Energy Rep.*, vol. 9(supl. 3), pp. 286–294, 2023, doi: 10.1016/j.egyr.2022.12.130.

[15] M. Pham, J. Kim, and C. Kim, "Rolling Bearing Fault Diagnosis Based on Improved GAN and 2-D Representation of Acoustic Emission Signals," *IEEE Access*, vol. 10, pp. 78056–78069, 2022, doi: 10.1109/ACCESS.2022.3193244.

[16] J. Pacheco-Cherrez, J.A. Fortoul-Diaz, F. Cortes-Santacruz, L.M. Aloso-Valerdi, D.I. Ibarra-Zarate, "Bearing fault detection with vibration and acoustic signals: Comparison among different machine leaning classification methods," *Eng. Fail. Anal.*, vol. 139, p. 1065115, 2022, doi: 10.1016/j.engfailanal.2022.106515.

[17] J. Hu, Y. Yu, J. Yang, and H. Jia, "Research on the generalisation method of diesel engine exhaust valve leakage fault diagnosis based on acoustic emission," *Measurement*, vol. 210, p. 112560, 2023, doi: 10.1016/j.measurement.2023.112560.

[18] X. Huang, Z. Teng, Q. Tang, Z. Yu, J. Hua, and X. Wang, "Fault diagnosis of automobile power seat with acoustic analysis and retrained SVM based on smartphone," *Measurement*, vol. 202, p. 111699, 2022, doi: 10.1016/j.measurement.2022.111699.

[19] A. Choudhary, R.K. Mishra, S. Fatima, and B.K. Panigrahi, "Multi-input CNN based vibro-acoustic fusion for accurate fault diagnosis of induction motor," *Eng. Appl. Artif. Intell.*, vol. 120, p. 105872, 2023, doi: 10.1016/j.engappai.2023.105872.

[20] T. He, S. Zhu, H. Wang, J. Wang, and T. Qing, "The diagnosis of satellite flywheel bearing cage fault based on two-step clustering of multiple acoustic parameters," *Measurement*, vol. 201, p. 111683, 2022, doi: 10.1016/j.measurement.2022.111683.

[21] S. Wu, J. Zhou, and T. Liu, "Compound Fault Feature Extraction of Rolling Bearing Acoustic Signals Based on AVMD-IMVO-MCKD," *Sensors*, vol. 22, no. 18, p. 6769, 2022, doi: 10.3390/s22186769.

[22] K. Feng, J. Ji, Q. Ni, and M. Beer, "A review of vibration-based gear wear monitoring and prediction techniques," *Mech. Syst. Signal Process.*, vol. 182, p. 109605, 2023, doi: 10.1016/j.ymssp.2022.109605.

[23] Y. Xu, X. Yan, K. Feng, X. Sheng, B. Sun, and Z. Liu, "Attention-based multiscale denoising residual convolutional neural networks for fault diagnosis of rotating machinery," *Reliab. Eng. Syst. Saf.*, vol. 226, p. 108714, 2022, doi: 10.1016/j.ress.2022.108714.

[24] Y. Zhang *et al.*, "Integrated intelligent fault diagnosis approach of offshore wind turbine bearing based on information stream fusion and semi-supervised learning," *Expert Syst. Appl*, vol. 232, p. 120854, 2023, doi: 10.1016/j.eswa.2023.120854.

[25] J. Bang, P. Di Marco, H. Shin, and P. Park, "Deep Transfer Learning-Based Fault Diagnosis Using Wavelet Transform for Limited Data". *Appl. Sci.*, vol. 12, p. 7450, 2022, doi: 10.3390/app12157450.

[26] J. Li, L. Ke, Q. Du, X. Ding, and X. Chen, "Research on the Classification of ECG and PCG Signals Based on BiLSTM-GoogLeNet-DS". *Appl. Sci.*, vol. 12, p. 11762, 2022, doi: 10.3390/app122211762.

[27] S. Iqbal, S.S. Naqvi, H.A. Khan, A. Saadat, and T.M. Khan, "G-Net Light: A Lightweight Modified Google Net for Retinal Vessel Segmentation". *Photonics*, vol. 9, p. 923, 2022, doi: 10.3390/photonics9120923.

[28] X. Yu and X. Li, "Sound Recognition Method of Coal Mine Gas and Coal Dust Explosion Based on GoogLeNet". *Entropy*, vol. 25, p. 412, 2023, doi: 10.3390/e25030412.

[29] X. Feng, X. Gao, and L. Luo, "A ResNet50-Based Method for Classifying Surface Defects in Hot-Rolled Strip Steel". *Mathematics*, vol. 9, p. 2359, 2021, doi: 10.3390/math9192359.

[30] G. Chakrapani and V. Sugumaran, "Transfer learning based fault diagnosis of automobile dry clutch system," *Eng. Appl. Artif. Intell.*, 117(Part A), p. 105522, 2023, doi: 10.1016/j.engappai.2022.105522.

[31] P. Khanna, M. Sahu, B.K. Singh, and V. Bhateja, "Early prediction of pathological complete response to neoadjuvant chemotherapy in breast cancer MRI images using combined Pre-trained convolutional neural network and machine learning," *Measurement*, vol. 207, p. 112269, 2023, doi: 10.1016/j.measurement.2022.112269.

[32] M.T. Fang, Z.J. Chen, K. Przystupa, T. Li, M. Majka, and O. Kochan, "Examination of Abnormal Behavior Detection Based on Improved YOLOv3," *Electronics*, vol. 10, no. 2, p. 197, 2021, doi: 10.3390/electronics10020197.

[33] J. Gajewski and D. Valis, "Verification of the technical equipment degradation method using a hybrid reinforcement learning trees-artificial neural network system," *Tribol. Int.*, vol. 153, p. 106618, 2021, doi: 10.1016/j.triboint.2020.106618.